ADVANCED MATERIALS
www.advmat.de

www.MaterialsViews.com

Core–Shell Structured High-*k* Polymer Nanocomposites for Energy Storage and Dielectric Applications

Xingyi Huang and Pingkai Jiang**

High-*k* polymer nanocomposites have considerable potential in energy storage and dielectric applications because of their ease of processing, flexibility, and low cost. Core–shell nanoarchitecture strategies are versatile and powerful tools for the design and synthesis of advanced high-*k* polymer nanocomposites. Recent and in-progress state-of-the-art advancements in the application of core–shell nanoarchitecture strategies to design and prepare high-*k* polymer nanocomposites are summarized. Special focus is directed to emphasizing their advantages over conventional melt-mixing and solution-mixing methods: first, homogeneous nanoparticle dispersion can be easily achieved even in highly loaded nanocomposites; second, the dielectric constant of the nanocomposites can be effectively enhanced and meanwhile the high breakdown strength can be well-preserved; third, for nanocomposites filled with electrically conductive nanoparticles, dielectric loss can be effectively surpressed, and meanwhile a high dielectric constant can be achieved. In addition, fundamental insights into the roles of the interfaces on the dielectric properties of the nanocomposites can be probed. The last part of the article is concluded with current problems and future perspectives of utilizing the core–shell nanoarchitecture strategies for the development of high-*k* polymer nanocomposites.

1. Introduction

High-dielectric-constant (high-*k*) materials have numerous applications in organic field-effect transistors (OFETs),[1–5] organic thin-film electroluminescent devices,[6] electrical stress control applications,[7–10] actuators,[11,12] and energy storage devices.[13–17] Taking electrical stress control as a typical example, **Figure 1** demonstrates the application of high-*k* materials. In power cable terminations, the shield layer finishes short of the insulated conductors and the electric field concentrates at the cutback points, resulting in a stressed field along the insulation surface beyond the shield layer. If the stressed field is out of control to cause breakdown of air, surface discharge occurs and this eventually leads to insulation failure, followed by cable breakdown. High-*k* materials can remarkably reduce the surface electric stress and keep it below the breakdown strength of air, which may eliminate the surface discharge eventually. An ideal high-*k* material will not only have a high dielectric constant but also will display low dielectric loss, high breakdown strength, and good processability. Organic polymers usually have a high breakdown strength and ease of processing, but most have a low dielectric constant (e.g., approximately 2 to 5). Although several have relatively high dielectric constants, their dielectric loss is usually high, particularly under high electric fields.[4] Dielectric ceramics, such as $BaTiO_3$, not only have giant dielectric constants ranging from several hundreds to tens of thousands, but also have low breakdown strength and/or high dielectric loss.[18] In addition, their poor processability and lack of flexibility also significantly limit their application. Overall, it is difficult to find a single material combining all the desirable properties for practical applications. Therefore, it is reasonable to believe that an effective approach to advanced high-*k* materials is to harness the advantages of both polymers and ceramics.

Compared with microsized particles, nanoparticles have larger interacting areas with the polymer matrix and thus have the potential to produce substantially higher polarization levels, breakdown strengths and mechanical enhancements, offering greater possibilities to tailor and optimize the properties of polymer nanocomposites. In addition, the small size of the nanoparticles makes it possible to reduce the dimensions of polymer nanocomposite-based devices, which is extremely important for the continuing miniaturization of electronic devices. Taking embedded planar capacitors as an example, the dielectric film should be thin enough to yield a high capacitance; this is typically achieved with micrometer scale films. On this scale, the capacitance density of the composite films significantly decreases with an increase in the high-*k* particle size from 100 nm to 2 μm.[19] Considering these factors, nanoparticles represent the optimal choice.

Although the utilization of nanoparticles offers many advantages for designing high-*k* polymer composites, there are many

Dr. X. Huang, Prof. P. Jiang
Department of Polymer Science and Engineering
Shanghai Key Lab of Electrical
Insulation and Thermal Aging
Shanghai Jiao Tong University
Shanghai 200240, PR China
E-mail: xyhuang@sjtu.edu.cn; pkjiang@sjtu.edu.cn

DOI: 10.1002/adma.201401310

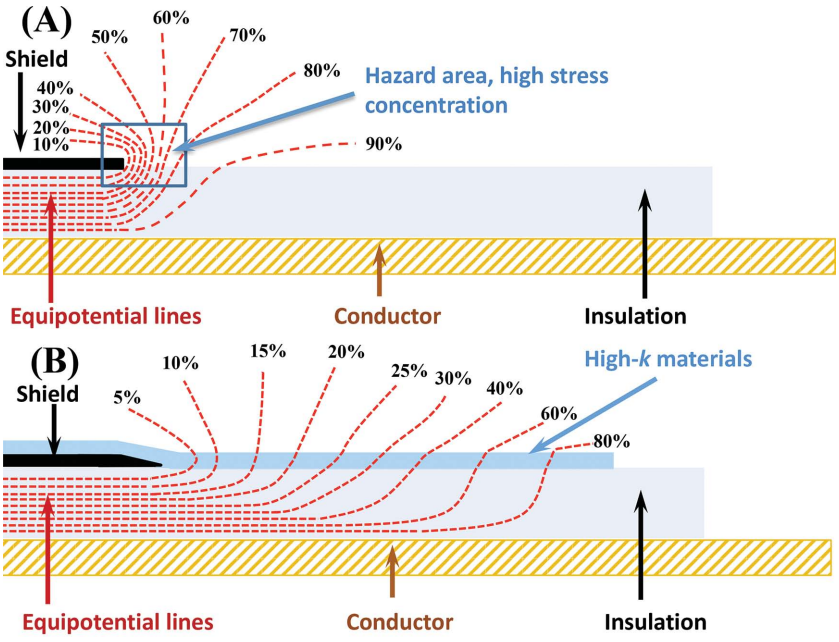

Figure 1. Electric stress and potential distribution at cable terminations without (A) and with (B) high-*k* material. The dashed lines are equipotential lines. Reproduced with permission.[9] Copyright 2014, Institute of Electrical and Electronics Engineers.

challenges in realizing high performance nanocomposites. Typical challenges include the realization of homogeneous nanoparticle dispersions and the tailoring of polymer/nanoparticle interfaces, which play key roles in achieving desirable electrical and other properties. Nanoparticle surface modification by hydroxylation,[20] coupling agents,[21] surfactants,[22,23] phosphoric acids[24,25] and other organic molecules[26] has been intensively used to improve the performance of high-*k* polymer nanocomposites. However, these methods still have some limitations in realizing the full potential of high-*k* polymer nanocomposites because the modifiers themselves usually do not play a significant role in the property enhancement of the nanocomposites.

To realize the full potential of nanoparticles to enhance the properties of polymer nanocomposites, significant efforts have recently been devoted to the design and synthesis of core–shell nanoparticles. Taking $BaTiO_3$ as an example, **Figure 2** presents some general methods for preparing high-*k* polymer nanocomposites using core–shell strategies. These methods can be categorized into four strategies: i) direct use of core–shell nanoparticles prepared by "grafting from";[27–29] ii) direct use of core–shell nanoparticles prepared by "grafting to";[30–33] iii) using core–shell organic–inorganic nanoparticles as fillers;[34,35] and iv) using other types of core–shell nanoparticles as fillers.[36–41]

This Research News article mainly reviews these emerging methods. Achieving a suitable balance between the dielectric constant, dielectric loss, and breakdown strength is critical to the successful application of high-*k* polymer nanocomposites.[42–44] Therefore, emphasis is placed on the merits of core–shell strategies in realizing low dielectric loss and high breakdown strength while maintaining the high dielectric constant of the nanocomposites.

2. Core–Shell Strategies for High-*k* Polymer Nanocomposites

2.1. Core–Shell Nanoparticles Prepared by the "Grafting-From" Route

This strategy relies on the formation of nanocomposites by the in situ polymerization of monomers on initiator-functionalized nanoparticle surfaces. The key to this strategy is the introduction of a sufficient quantity of initiating sites on the nanoparticle surfaces. Controlled/living radical polymerization, such as atom transfer radical polymerization (ATRP) and reversible addition-fragmentation chain transfer (RAFT) polymerization, is a feasible and powerful "grafting from" technique[27–29,34] providing many advantages: i) the shell layer coated on the nanoparticle surfaces prevents nanoparticle aggregation; ii) the nanocomposites can be formed directly from core–shell nanoparticles using the shell layer as a matrix, which allows the preparation of high-quality, highly filled nanocomposites (e.g., free of defects, such as voids and pores); iii) any polymer chains are robustly bonded on the nanoparticle surfaces, resulting in a strong nanoparticle/matrix interface; iv) the nanoparticle concentration can be adjusted by tuning the feed ratio of the monomer and the initiator functionalized nanoparticles; v) there is a broad range of monomers that can be polymerized.

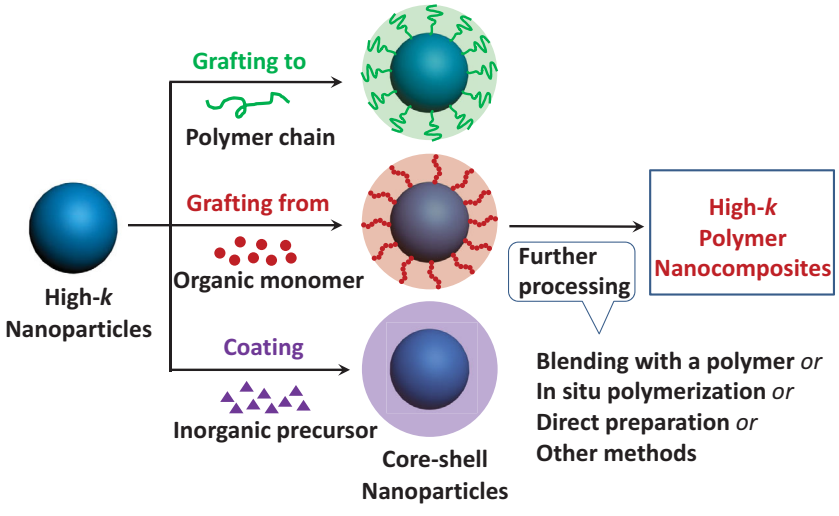

Figure 2. General methods associated with the design and construction of core–shell nanoparticles for high-*k* polymer nanocomposites.

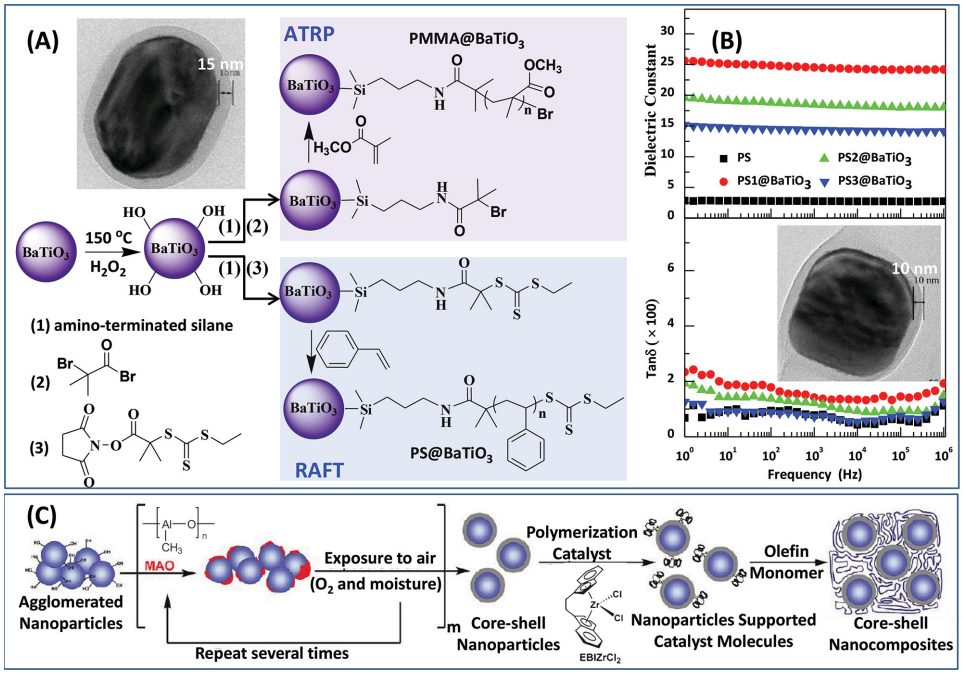

Figure 3. A) Illustration of the synthesis routes for high-*k* poly(methyl methacrylate) [PMMA] and polystyrene (PS) nanocomposites by ATRP and RAFT polymerization, respectively. The inset in (A) shows a TEM image of core–shell PMMA@$BaTiO_3$. Reproduced with permission.[28] Copyright 2011, Royal Society of Chemistry. B) Frequency dependent dielectric properties of the PS@$BaTiO_3$ nanocomposites. The inset in (B) shows a TEM image of core–shell PS@$BaTiO_3$. Reproduced with permission.[29] Copyright 2012, Wiley-VCH. C) Illustrations of the synthesis routes of ^{iso}PP nanocomposites. Reproduced with permission.[32] Copyright 2010, American Chemical Society.

Huang and Jiang have used ATRP and RAFT to prepare core–shell high-*k* PMMA@$BaTiO_3$ and PS@$BaTiO_3$ nanocomposites, respectively, as shown in **Figure 3**A.[28,29] Homogeneous nanoparticle dispersion was observed in both types of highly filled nanocomposites. Taking the PS@$BaTiO_3$ nanocomposites as an example (see Figure 3B), the dielectric constant of the nanocomposite with ca. 48 vol% $BaTiO_3$ increased to 24 from the value of 2.8 observed for the pure PS, while the dielectric loss had nearly the same inherently low value as the pure PS. More importantly, the dielectric constant and dielectric loss were stable over a wide range of frequencies, which is very useful for functional devices that demand insensitive operation over wide ranges of frequency.

Biaxially oriented polypropylene (BOPP) film based capacitors have been widely used in consumer electronics, electrical vehicles, electric grids, and pulse-power systems because of their unique combination of properties, including a low energy loss, high breakdown strength, low capacity loss under high frequencies, sealability, lightweight and flexibility. However, the low dielectric constant of PP limits the utilization of BOPP in future applications that might demand the rapid delivery of large bursts of energy. In 2007, the Marks research group has reported an effective method for the preparation of PP based high-*k* and low loss nanocomposites.[32,45–49] In this method, the nanoparticles (e.g., $BaTiO_3$, TiO_2, ZrO_2, $SrTiO_3$, MgO, $Ba_{0.5}Sr_{0.5}TiO_3$, Al) were first coated with a methylaluminoxane (MAO) co-catalyst (Figure 3C), which allowed the formation of covalent Al-O bonding. Then, the MAO treated nanoparticles were subjected to reaction with a metallocene olefin polymerization catalyst, [ac-ethylenebisindenyl]zirconium dichloride ($EBIZrCl_2$). The functionalization of the MAO-treated nanoparticles by $EBIZrCl_2$ resulted in polymerization-active species anchored on the nanoparticle surfaces that could initiate the in situ propylene polymerization and finally yield isotactic PP (^{iso}PP) nanocomposites. The prepared ^{iso}PP nanocomposites had a higher dielectric constant and sufficiently high breakdown strength and thus exhibited significantly enhanced energy storage capacity compared with pure PP. Although only a few monomers are suitable for this method, it has several unique merits: i) the nanocomposites can be produced on a huge scale; ii) the growth of the propagating polyolefin chains from the activated catalyst centers can result in large local hydrostatic pressures, which may disrupt nanoparticle aggregation in the final nanocomposites; and iii) more importantly, this method provides an effective way to minimize the electrical mismatch between the nanoparticles and the matrix. In particular, the nanoparticles are coated with a substance (i.e., Al_2O_3) that has a dielectric constant greater than that of the matrix but lower than that of the nanoparticles. Recalling that the decrease in breakdown strength of high-*k* polymer composites with ceramics mainly originates from the large dielectric constant mismatch, the introduction of Al_2O_3 may be beneficial in maintaining the high breakdown strength of the nanocomposites. In fact, a high breakdown strength was obtained in Al-^{iso}PP nanocomposites.[48] As reported by Marks, even at a high metal nanoparticle concentration (i.e., 12.4 vol%), the Al-^{iso}PP nanocomposites have a high breakdown strength of nearly 80 MV m^{-1}. Because of the electrical conduction due to interparticle tunneling, the conductive particle filled polymer composites generally exhibit a very low breakdown strength, even

when the particle concentration is far below the percolation threshold.[50] Here, the high breakdown strength of the ^{iso}PP nanocomposites with a high loading of Al nanoparticles may be attributed to the surface coating of Al by Al_2O_3, which inhibits the tunneling current between particles.

2.2. Core–Shell Nanoparticles Prepared by the "Grafting-To" Method

This strategy involves the formation of nanocomposites by grafting the pre-prepared polymer chains onto the nanoparticles surface via a reaction between the polymer end-groups and the functional groups on the nanoparticle surfaces. Compared with the "grafting from" strategy, the "grafting to" strategy allows us to control the molecular composition and the molecular weight of the polymer chains according to the desired performance of the final nanocomposites.

Click chemistry is a universal method used to link reaction partners and has the advantages of high efficiency, solvent insensitivity and moderate reaction conditions. Therefore, click reactions are a versatile method for the grafting of polymer chains to nanoparticle surfaces. Tchoul and Vaia prepared a series of core–shell PS@TiO_2 nanocomposites by a Cu(I)-catalyzed alkyne–azide click (CuAAC) reaction.[30] The dielectric constant of the core–shell PS (100 kg mol^{-1}) nanocomposites with 27 vol% TiO_2 was 6.4 at 1000 Hz, while the dielectric loss tangent was as low as 0.625%. The nanocomposite can be used as the gate dielectric in thin-film-transistor based on organic semiconductors to achieve high carrier mobility and low leakage current.[31] The disadvantage of the CuAAC reaction is that the catalyst, CuBr, cannot be easily removed from the nanocomposites because of its strong complexation with azides and triazoles, which may cause strong frequency dependent dielectric properties and high dielectric loss.

Unlike the CuAAC reaction, the thiol-ene click reaction is not only highly efficient and free of byproducts but also does not require catalysis by transition metals. Therefore, the thiol-ene click reaction is much more suitable for the preparation of core–shell structured polymer nanocomposites. Huang and Jiang reported a thiol-ene reaction route to core–shell polymer@$BaTiO_3$ nanocomposites; the preparation process is illustrated in **Figure 4**A.[51] Thiol-terminated PS or PMMA macromolecular chains with different molecular weights were first prepared by RAFT polymerization, and core–shell polymer@$BaTiO_3$ nanoparticles were fabricated by grafting the macromolecular chains on the surface of vinyl-functionalized $BaTiO_3$ nanoparticles via the thiol-ene click reaction. The nanocomposites showed a significantly enhanced dielectric constant, while their dielectric loss was still as low as that of the pure polymer, except at super-low frequencies. This investigation also demonstrated that the dielectric properties, in particular the dielectric loss, of the core–shell polymer@$BaTiO_3$ nanocomposites were dependent on the molecular weight of the polymer chains and the grafting density of the core–shell structured nanoparticles, in particular at low frequencies (see Figure 4D,E).

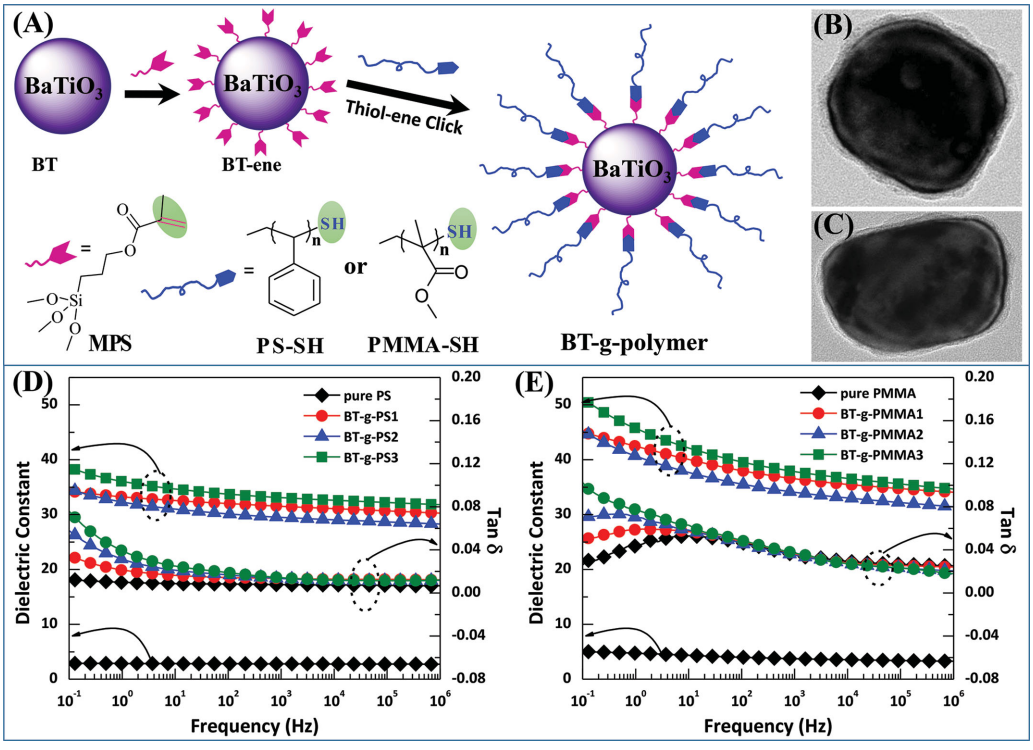

Figure 4. A) Illustrations of the synthesis process for PS@$BaTiO_3$ and PMMA@$BaTiO_3$ nanocomposites by thiol-ene click reactions. B,C) TEM images of core–shell PS@$BaTiO_3$ (B) and PMMA@$BaTiO_3$ (C). D,E) Frequency-dependent dielectric constant and tan delta for PS@$BaTiO_3$ (D) and PMMA@$BaTiO_3$ (E) nanocomposites. The calculated molecular weights of PS1, PS2 and PS3 were 10.3, 41.6 and 80.5 kg mol^{-1}, respectively. The calculated molecular weights of PMMA1, PMMA2 and PMMA3 were 10.7, 42.6 and 81.3 kg mol^{-1}, respectively. Reproduced with permission.[51] Copyright 2014, American Chemical Society.

In general, polymer chains with high molecular weights tend to result in low grafting density and thus high dielectric loss in the nanocomposites.

Apart from the click reaction, any other linking reaction between organic molecular chains and nanoparticle surfaces can also be used to prepare core–shell structured high-*k* nanocomposites. Toward high-*k* flexible gate dielectrics for organic semiconductor thin-film-transistors, Maliakal et al. successfully prepared core–shell high-*k* PS@TiO_2 nanocomposite dielectrics by attaching phosphonate end functionalized PS to oleic acid terminated TiO_2 nanoparticle surfaces.[31] The nanocomposites showed a high dielectric constant of 9.4 when the TiO_2 was at 18.2 vol%, and the resulting transistor exhibited desirable high mobility. Jung and Kim prepared core–shell high-*k* nanoparticles by wrapping $BaTiO_3$ with a polystyrene-*block*-poly(styrene-*co*-vinylbenzylchloride) [PS-b-PSVBC] copolymer, resulting in a unique core–shell structure in which the charged PSVBC was shielded by the PS shell. In this case, the charged PSVBC shell enhanced the dielectric constant, while the PS shell suppressed the leakage current and minimized the development of breakdown paths. The increase of the dielectric constant originates from the enhanced interfacial polarization between the PS shell and the PSVBC shell. The suppressed leakage currents and the enhanced breakdown strength should be attributed to the shielding of charge-rich PSVBC shell by the PS shell. The nanocomposites showed a significantly enhanced energy storage density and the maximum theoretical energy density of 9.7 J cm^{-3} was observed in the PS-b-PSVBC nanocomposites containing 75 wt% $BaTiO_3$.[33]

For the large-scale preparation of high-*k* nanocomposites, the use of commercially available polymers as shells is more attractive. In a recent study, by using the "grafting to" strategy, Huang and Jiang prepared core–shell high-*k* polymer@$BaTiO_3$ nanocomposites using commercially available poly(vinylidene fluoride-*co*-hexafluoropropylene) [PVDF-HFP] modified with poly(glycidyl methacrylate) [PGMA].[52] The PGMA functionalized PVDF-HFP formed a robust and stable shell on the $BaTiO_3$ surfaces, resulting in a homogeneous dispersion of $BaTiO_3$ nanoparticles in PVDF-HFP. In addition, the dielectric constant and energy density of the nanocomposites were enhanced as the $BaTiO_3$ concentration increased, while the dielectric loss showed a slight decrease with increasing $BaTiO_3$ content.

2.3. Core–Shell Organic–Inorganic Nanoparticles as Fillers

Like the conventional melt-mixing and solution-mixing methods for composite preparation, this approach corresponds to the preparation of nanocomposites by introducing core–shell organic–inorganic nanoparticles into a polymer matrix. One of the main merits of this method is that one can precisely control the inorganic nanoparticle concentration in the nanocomposites and the properties closely associated with the nanoparticle concentration. More importantly, this approach allows us to obtain fundamental insights into the role of the interface on the electrical properties of the nanocomposites.

Huang and Jiang investigated the role of shell/matrix physical interaction on the dielectric properties of nanocomposites composed of ferroelectric polymers and core–shell fluoro-polymer@$BaTiO_3$ nanoparticles.[34] The authors first prepared core–shell fluoro-polymer@$BaTiO_3$ nanoparticles not only with different shell thicknesses but also with different shell molecular structures by grafting two types of fluoroalkyl acrylate monomers (1H,1H,2H,2H heptadecafluorodecyl acrylate, HFDA, and trifluoroethyl acrylate, TFEA) via surface-initiated RAFT polymerization. Then, the nanocomposites were prepared by adding the fluoro-polymer@$BaTiO_3$ nanoparticles to P(VDF-HFP). The authors found that the dielectric properties and energy storage capability of the nanocomposites were closely associated with the shell structure of the fluoro-polymer@$BaTiO_3$. As shown in **Figure 5**A, the authors suggested that the ordered chain structure of PHFDA caused low chain mobility and low interchain interactions between PHFDA@$BaTiO_3$ and the PVDF-HFP matrix, while the disordered chain structure of PTFEA caused high chain mobility and high interchain interactions between PTFEA@$BaTiO_3$ and the PVDF-HFP matrix, resulting in stronger suppression of the space charge polarization and a larger restriction of the dipole movement of the P(VDF-HFP) matrix. As a consequence, a lower dielectric loss, higher breakdown strength, and stronger energy storage capability were achieved in the PTFEA@$BaTiO_3$ nanocomposites.

Huang and Jiang also investigated the role of the shell/matrix chemical interaction (i.e., interfacial bonding) on the dielectric properties of high-*k* polymer nanocomposites. For this purpose, they made a comparative investigation of the dielectric properties of single-core@double-shell nanocomposites (Nanocomposite I) and single-core@single-shell nanoparticle filled nanocomposites (Nanocomposite II). Here, the outer shell of Nanocomposite I had the same chemical structure as the matrix of Nanocomposite II.[53] They first prepared single-core@single-shell nanoparticles (termed HBP@$BaTiO_3$) by growing hyperbranched aromatic polyamides (HBP) on the $BaTiO_3$ nanoparticle surfaces. Then, they prepared Nanocomposite I (i.e., PMMA@HBP@$BaTiO_3$) by growing PMMA on the surface of HBP@$BaTiO_3$ nanoparticles via ATRP. Nanocomposite II (PMMA/HBP@$BaTiO_3$) was prepared by blending the core–shell HBP@$BaTiO_3$ nanoparticles with PMMA.[53] Both nanocomposites exhibited homogeneous nanoparticle dispersion and good interfacial adhesion. However, dielectric characterization showed that the two types of nanocomposites exhibited significantly different properties. The PMMA@HBP@$BaTiO_3$ nanocomposites were highly electrically insulating, exhibiting low electrical conductivities at low frequencies, strongly frequency dependent electrical conductivities and weakly frequency dependent dielectric parameters. In this case, their high dielectric constant makes them very attractive for power energy storage and gate-dielectric applications. The highly loaded PMMA/HBP@$BaTiO_3$ nanocomposites, however, showed dielectric properties similar to those of percolative composites. Namely, the nanocomposites exhibited frequency-independent electrical conductivity, and both the dielectric constant and dielectric loss were significantly enhanced at low frequencies and decreased rapidly with increasing frequency. In spite of the very high dielectric constant achieved, the high electrical conductivities and dielectric loss make the PMMA/HBP@$BaTiO_3$ nanocomposites unattractive in any power energy storage and dielectric application. In another research work,

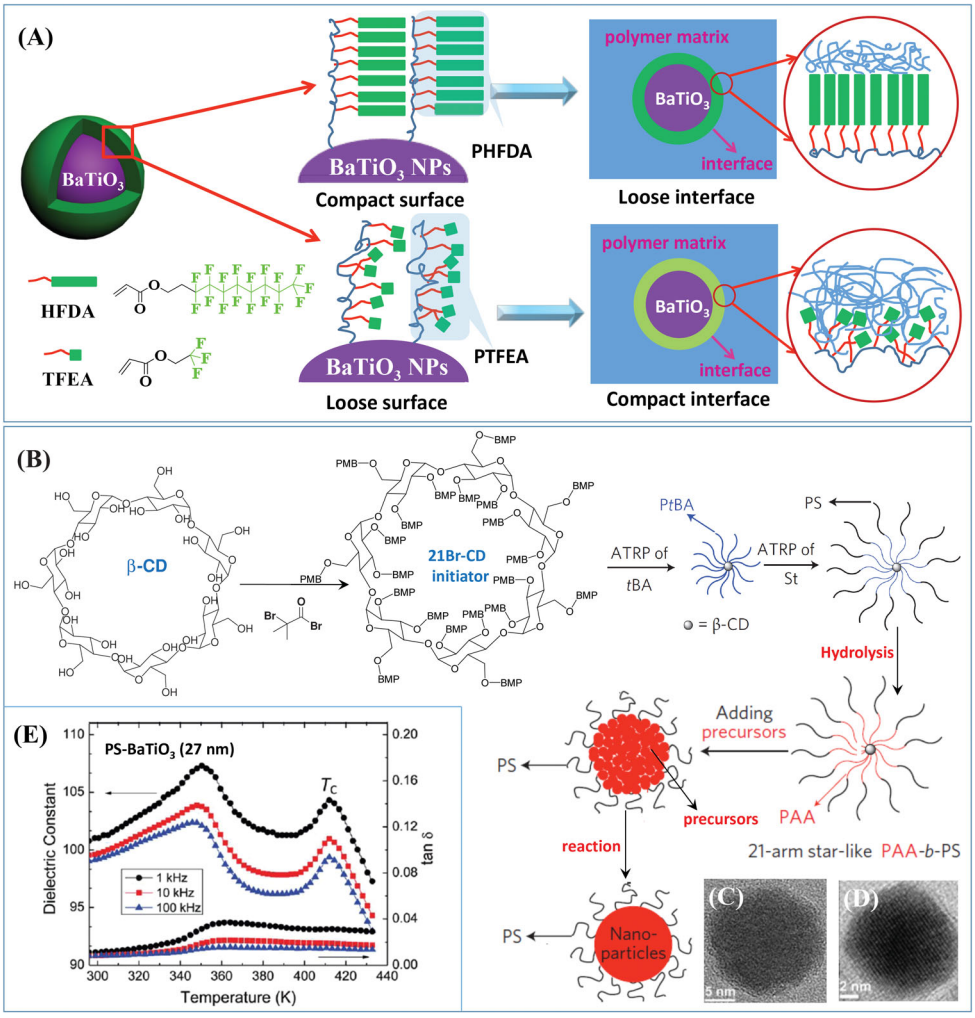

Figure 5. A) Illustrations of the interface in fluoro-polymer@$BaTiO_3$ nanocomposites. Reproduced with permission.[34] Copyright 2013, American Chemical Society. B) Illustrations of the synthesis process for the core–shell PS@$BaTiO_3$ nanoparticle. Reproduced with permission.[55] Copyright 2013, Macmillan Publisher Limited. C,D) TEM images of $BaTiO_3$ nanoparticles with an average diameter of 27 nm (C) and 11 nm (D). C,D) Reproduced with permission.[35] Copyright 2013, Royal Society of Chemistry. E) Temperature dependence of the dielectric constant and dielectric loss of PS@$BaTiO_3$ (27 nm) nanoparticle compact. Reproduced with permission.[56] Copyright 2012, Royal Society of Chemistry.

Huang and Jiang prepared fluoro-tripolymer/HBP@$BaTiO_3$ blends in which the core–shell HBP@$BaTiO_3$ nanoparticles were incompatible with the fluoro-tripolymer matrix.[54] The authors found that, at relatively high HBP@$BaTiO_3$ concentrations (i.e., higher than 20 vol%), the composites began to display dielectric properties similar to those of percolative composites.

The aforementioned two studies indicate that, when a matrix and the introduced inclusion have large electrical conductivity mismatch, the formation of interfacial bonding usually is the key factor to achieving desirable dielectric properties in the composites. In the case of the single-core@double-shell nanocomposites, the outer shell covalently bonded with the inner shell was able to block the movement of charge carriers through the nanocomposites by playing a shielding role on the charge-rich inter layer, which resulted in weak interfacial polarization and low leakage current density and thus improved the dielectric properties (e.g., low dielectric loss).

To date, the majority of the core–shell polymer@$BaTiO_3$ reported in the literature have been based on commercially available $BaTiO_3$ nanoparticles, which is a relatively feasible and potentially timesaving approach. However, these methods fail to control the nanoparticle size and thus their size-dependent electrical properties. More recently, Lin's group reported an interesting general strategy to prepare core–shell nanoparticles, including the core–shell polymer@$BaTiO_3$.[55,56] As shown in Figure 5B, they first prepared star-like giant molecules by growing poly(acrylic-acid)-*block*-polystyrene (PAA-b-PS) from a β-cyclodextrin core via ATRP and hydrolysis. They then introduced the inorganic precursor and made the precursor accumulate in the hydrophilic core (PAA) of the PAA-b-PS by choosing a proper solvent. Finally, $BaTiO_3$ single crystalline nanoparticles with the same size as the PAA core were fabricated by condensation at high temperatures. This approach allowed the control of the $BaTiO_3$ single crystalline nanoparticle size by controlling the size of the PAA core. Two types of core–shell nanoparticles

with different $BaTiO_3$ sizes (27 nm and 11 nm) were successfully fabricated (Figure 5C,D) and were found to exhibit much higher dielectric constants (Figure 5E) than those of previously reported core–shell nanocomposites prepared by commercially available $BaTiO_3$ nanoparticles (in most cases, the size was approximately 50–140 nm).[35,55] The low dielectric loss (Figure 5E) of the high-*k* nanocomposites demonstrated their promising potential for energy storage and dielectric applications. Interestingly, the core–shell nanoparticles were also used as fillers to prepare diblock copolymer (PS-b-PMMA) based high-*k* polymer nanocomposites. In contrast to the nanocomposites prepared by traditional blending methods, in which the nanoparticles are randomly dispersed in a polymer matrix, the PS@$BaTiO_3$ were selectively introduced into the cylindrical PS nanodomains in PS-b-PMMA, resulting in vertically oriented PS nanocylinders loaded with PS@$BaTiO_3$ in the final nanocomposites. Even in the high frequency range (i.e., 2–15 GHz), the PS-b-PMMA/PS@$BaTiO_3$ nanocomposites showed frequency-independent high dielectric constants (>18) and low dielectric loss,[35] also showing great potential for energy storage and dielectric applications.

2.4. Other Types of Core–Shell Nanoparticles as Fillers

Apart from core–shell structured inorganic–organic nanoparticles, other types of core–shell structured nanoparticles have also been used as fillers to prepare high-*k* polymer nanocomposites, including inorganic–inorganic (e.g., TiO_2@$BaTiO_3$ and SiO_2@$BaTiO_3$),[36,57] metal–inorganic (e.g., Al_2O_3@Al and TiO_2@Ag),[37,41] metal–organic (e.g., C@Ag) and organic–organic (e.g., polydivinylbenene@polyaniline, PDVB@PANI) hybrids.[39,40,58]

Yao and Rahimabady prepared core–shell structured TiO_2@$BaTiO_3$ nanoparticles and corresponding PVDF nanocomposites.[57] They surprisingly found that, compared with the PVDF/$BaTiO_3$ nanocomposites, the PVDF/TiO_2@$BaTiO_3$ nanocomposites showed significantly improved dielectric properties. Specifically, both the dielectric constant and the breakdown strength were increased in the PVDF/TiO_2@$BaTiO_3$ nanocomposites. The nanocomposite with 30 vol% TiO_2@$BaTiO_3$ had a discharged energy density of 12.2 J cm^{-3} at 340 MV m^{-1}, nearly 3 times that of pure PVDF (4.1 J cm^{-3}). It has been widely accepted from previous research that the significant increase in dielectric constants observed in polymer nanocomposites filled with high-*k* particles is usually achieved at the expense of a decrease in breakdown strength. From this viewpoint, the research of Yao and Rahimabady provides an important clue to resolve this well-known contradiction. The authors attributed the dielectric performance enhancement to the introduction of a TiO_2 layer, which reduced the local electric field distortion. This is generally consistent with the "buffer layer" model proposed by the Marks group. Wong and Xu have pioneered the preparation of low-loss, high-*k* polymer nanocomposites using core–shell structured Al_2O_3@Al nanoparticles.[37] It has been reported that the dielectric constant is as high as 60 when the Al nanoparticle (approximately 100 nm) fraction is 50 wt%, while the dielectric loss is as low as 0.02. The electrically conductive Al core results in electric field enhancement in the polymer matrix, which contributes to the increase in the dielectric constant of the nanocomposites. The electrically insulating Al_2O_3 layer outside of the Al core restricts electron transfer between the Al nanoparticles, resulting in low dielectric loss.

Ag is a good conductor of electricity, enabling Ag filled polymer composites to act as typical percolation systems, in which the dielectric constant of the composites increases slowly with the Ag particle loading far below the percolation threshold and increases rapidly near the percolation threshold. Finally, the composites become electrically conductive beyond the percolation threshold, and then the dielectric constant exhibits an abrupt decrease.[17] Once the Ag nanoparticles are encapsulated by an insulating polymer shell, the formation of conductive paths by direct contact between the Ag nanoparticles is hindered, and the tunneling currents between neighboring Ag nanoparticles decreases with increasing shell thickness. When the shell thickness increases to a critical value at which the tunneling current becomes negligible, the nanocomposites filled with insulating shell encapsulated Ag become insulating, even though the Ag content is high. In this case, the nanocomposites will simultaneously exhibit a high dielectric constant and low dielectric loss. Shen and Nan found that the dielectric constant of an epoxy nanocomposite filled with core–shell C@Ag nanoparticles increased by more than two orders of magnitude when the Ag nanoparticle concentration was larger than 20 vol%, while the dielectric loss tangent only showed a small increase (i.e., from 2% to 4%).[39,40] In addition, it also should be noted that the dielectric properties of the epoxy/C@Ag nanocomposites can be tuned by the shell thickness.

When the diameter of a nanocrystal decreases to a small enough size (i.e., the wavelength of the electron wave function), quantum confinement and coulomb blockade effects may occur.[59] In this case, a metallic particle can become electrically insulating. In addition, the transfer of electrons from a particle to its neighboring particle will be blocked. In this context, one may utilize the quantum confinement and coulomb blockade effects of ultra-small metallic nanoparticles to suppress leakage current and to increase the breakdown strength of high-*k* nanocomposites. Indeed, Xie and Huang found that, in comparison with $BaTiO_3$ nanocomposites, nanocomposites filled with ultra-small-Ag decorated $BaTiO_3$ (core-satellite such as Ag@$BaTiO_3$) hybrid nanoparticles showed decreased dielectric loss and enhanced breakdown strength.[38] The authors indirectly elucidated the existence of a coulomb blockade effect in the Ag@$BaTiO_3$ nanocomposites according to the significantly decreased electrical conductivities.

Inorganic and metal core based core–shell nanoparticles generally have a high density, which may lead to heaviness in the target devices. To decrease the device weight but maintain the device performance, the utilization of all-organic fillers is welcome. Toward this aim, Molberg and Opris prepared high-*k* polydiomethylsiloxane (PDMS) nanocomposites by using polydivinylbenzene encapsulated polyaniline (PDVB@PANI) core–shell particles.[58] Surprisingly, compared with pure PDMS, the PDMS/PDVB@PANI composites not only showed increased dielectric constants but also had a comparable breakdown strength. For example, at 100 Hz, the dielectric constant increased to 7.6 for the composites with 31.7% PDVB@PANI nanoparticles from a value of 2.3 for pure PDMS, while the breakdown strength of the composites only showed a slight decrease (i.e., from 66.1 to 64.1 V μm^{-1}).

3. Summary and Outlook

Core–shell strategies are powerful and versatile tools for designing and preparing high-*k* polymer nanocomposites for energy storage and dielectric applications, providing opportunities to control and optimize the microstructure (e.g., nanoparticle dispersion) and the electrical properties of the nanocomposites by engineering the interface between the nanoparticles and the polymer matrix. Compared with conventional melt-mixing and solution-mixing methods for fabrication of high-*k* polymer nanocomposite, core–shell strategies have the following distinct advantages:

First, on one hand, the core–shell strategies enable the direct fabrication of high-*k* nanocomposites by pressing the core–shell nanoparticles together; on the other hand, through the srategies, it is possible to make the polymer shell and polymer matrix possess similar chemical structures, which can result in homogeneous nanoparticle dispersion in the matrix even at a very high fraction of the nanoparticle (e.g., 50 vol%). This is crucial for fabrication of nanocomposites with high over-all performance.

Second, the core–shell strategies provide some intriguing approches to resolve the well-known paradoxes (i.e., nanocomposites with a high dielectric constant usually suffer from the low breakdown strength, high dielectric loss and high leakage currents), which cannot be well-solved by conventional melt-mixing and solution-mixing methods. For example, in single-core@multi-shell structured high-*k* nanoparticles, the dielectric constant of the shells shows a gradient decrease from the shell to the matrix. The shells act as buffer layers to minimize the local electric field enhancement, rendering enhanced breakdown strength of the nanocomposites. The other example is that, one can utilize the quantum confinement and coulomb blockade effects of ultra-small metallic nanoparticles decorated on the surface of high-*k* particles to suppress the leakage currents and increase the breakdown strength of the high-*k* nanocomposites.

Third, the core–shell strategies enable the disappearance of electrical percolation transition in polymer nanocomposites filled with electrically conductive particles, resulting in high dielectric constant, low dielectric loss and acceptable breakdown strength. The recent work of Marks's group revealed that,[48] even at a high metal nanoparticle concentration, the PP nanocomposites with Al_2O_3@Al core–shell nanoparticles simultaneously have a high breakdown strength (e.g., 75.8 MV m^{-1} for PP nanocomposites with 12.4 vol% Al_2O_3@Al core–shell nanoparticles), low dielectric loss and high dielectric constant. This is the first demonstration indicating metallic nanoparticles filled nanocomposites are adoptable and attractive for energy storage applications (e.g., the discharged energy density is 13.4 J/cm^3 for PP nanocomposites with 12.4 vol% Al_2O_3@Al core–shell nanoparticles).

Fourth, the core–shell strategies provide much more opportunities to significantly enhance the dielectric properties of the high-*k* nanocomposites when compared with the conventional melt-mixing and solution-mixing methods. For instance, the nanocomposites directly prepared by polymer@$BaTiO_3$ nanoparticles from the star-like unimolecular block copolymer micelles have much higher dielectric constant than those of nanocomposites ever reported fabricated by commercially available $BaTiO_3$ nanoparticles, while comparable low dielectric loss is kept.[56]

Fifth, the core–shell strategies allow us to easily control the critical factors which significantly influence the electrical properties of the high-*k* nanocomposites, including interface (shell) thickness, interface interactions and electrical mismatch at the interfaces etc. This provide an unique approach to achieve fundamental insights into the roles of the interfaces on the electrical properties of the high-*k* nanocomposites.

Although significant progress has been made in developing high-*k* nanocomposites for energy storage and dielectric applications by core–shell strategies, challenges still lie ahead, including the design and preparation of high-*k* nanocomposites simultaneously exhibiting a high breakdown strength, low dielectric loss and other desirable properties on a large scale of production while maintaining precise control over the nanoarchitectures of the core–shell nanoparticles. Technologically, the use of one-core@multi-shell strategies, the incorporation of nanoparticles having desirable nanoeffects in the shells and innovative synthesis technologies for core–shell nanoparticles may provide opportunities to overcome these limitations. Harnessing the opportunities of advanced high-*k* nanocomposites requires the efficient and close interdisciplinary cooperation between chemists, materials scientists and electrical engineers. Last but certainly not least, the processing detail and typical property requirements of high-*k* nanocomposites used in the real world are also important to inspire innovative ideas for the development of new advanced high-*k* nanocomposites, particularly for those in the academic community.

Acknowledgements

The authors gratefully acknowledge support from the National Natural Science Foundation of China (Nos. 51107081, 51277117) and the Special Fund of the National Priority Basic Research of China under Grant 2014CB239503. X.Y.H. thanks the SMC Excellent Young Faculty Award of Shanghai Jiao Tong University for finical support. This work was also sponsored by Shanghai Pujiang Program under Grant PJ14D018 in part (X.Y.H.). The authors also thank Ke Yang for the preparation of Figure 2.

Received: March 24, 2014
Revised: June 15, 2014
Published online: September 3, 2014

[1] R. P. Ortiz, A. Facchetti, T. J. Marks, *Chem. Rev.* **2010**, *110*, 205.
[2] J. H. Li, Z. H. Sun, F. Yan, *Adv. Mater.* **2012**, *24*, 88.
[3] Y. J. Kim, J. Kim, Y. S. Kim, J. K. Lee, *Org. Electron.* **2013**, *14*, 3406.
[4] S. K. Hwang, I. Bae, S. M. Cho, R. H. Kim, H. J. Jung, C. Park, *Adv. Funct. Mater.* **2013**, *23*, 5484.
[5] L. M. Huang, Z. Jia, I. Kymissis, S. O'Brien, *Adv. Funct. Mater.* **2010**, *20*, 554.
[6] Y. H. Chen, Y. D. Xia, H. D. Sun, G. M. Smith, D. Z. Yang, D. G. Ma, D. L. Carroll, *Adv. Funct. Mater.* **2013**, *24*, 1501.
[7] A. Eigner, S. Semino, *IEEE Electr. Insul. Mag.* **2013**, *29*, 47.
[8] Z. M. Dang, J. K. Yuan, J. W. Zha, T. Zhou, S. T. Li, G. H. Hu, *Prog. Mater. Sci.* **2012**, *57*, 660.

[9] X. Y. Huang, L. Y. Xie, K. Yang, C. Wu, P. K. Jiang, S. T. Li, S. Wu, K. Tatsumi, T. Tanaka, *IEEE Trans. Dielectr. Electr. Insul.* **2014**, *21*, 467.
[10] E. Sharifi, S. H. Jayaram, E. A. Cherney, *IEEE Trans. Dielectr. Electr. Insul.* **2010**, *17*, 264.
[11] Q. M. Zhang, V. Bharti, X. Zhao, *Science* **1998**, *280*, 2101.
[12] Q. M. Zhang, H. F. Li, M. Poh, F. Xia, Z. Y. Cheng, H. S. Xu, C. Huang, *Nature* **2002**, *419*, 284.
[13] Z. M. Dang, J. K. Yuan, S. H. Yao, R. J. Liao, *Adv. Mater.* **2013**, *25*, 6334.
[14] B. J. Chu, X. Zhou, K. L. Ren, B. Neese, M. R. Lin, Q. Wang, F. Bauer, Q. M. Zhang, *Science* **2006**, *313*, 334.
[15] M. A. Alam, M. H. Azarian, M. G. Pecht, *J. Mater. Sci. Mater. Electron.* **2012**, *23*, 1504.
[16] C. W. Nan, Y. Shen, J. Ma, *Ann. Rev. Mater. Res.* **2010**, *40*, 131.
[17] L. Zhu, Q. Wang, *Macromolecules* **2012**, *45*, 2937.
[18] M. Arbatti, X. B. Shan, Z. Y. Cheng, *Adv. Mater.* **2007**, *19*, 1369.
[19] R. N. Das, J. M. Lauffer, V. R. Markovich, *J. Mater. Chem.* **2008**, *18*, 537.
[20] J. J. Li, S. I. Seok, B. J. Chu, F. Dogan, Q. M. Zhang, Q. Wang, *Adv. Mater.* **2009**, *21*, 217.
[21] X. Y. Huang, L. Y. Xie, K. Yang, C. Wu, P. K. Jiang, S. T. Li, S. Wu, K. Tatsumi, T. Tanaka, *IEEE Trans. Dielectr. Electr. Insul.* **2014**, *21*, 480.
[22] H. Tang, Y. Lin, H. A. Sodano, *Adv. Energy Mater.* **2013**, *3*, 451.
[23] J. J. Li, P. Khanchaitit, K. Han, Q. Wang, *Chem. Mater.* **2010**, *22*, 5350.
[24] P. Kim, S. Jones, P. Hotchkiss, J. Haddock, B. Kippelen, S. Marder, J. Perry, *Adv. Mater.* **2007**, *19*, 1001.
[25] P. Kim, N. M. Doss, J. P. Tillotson, P. J. Hotchkiss, M. J. Pan, S. R. Marder, J. Y. Li, J. P. Calame, J. W. Perry, *ACS Nano* **2009**, *3*, 2581.
[26] P. H. Hu, Y. Shen, Y. H. Guan, X. H. Zhang, Y. H. Lin, Q. M. Zhang, C. W. Nan, *Adv. Funct. Mater.* **2014**, *24*, 3172.
[27] S. A. Paniagua, Y. S. Kim, K. Henry, R. Kumar, J. W. Perry, S. R. Marder, *ACS Appl. Mater. Interfaces* **2014**, *6*, 3477.
[28] L. Y. Xie, X. Y. Huang, C. Wu, P. K. Jiang, *J. Mater. Chem.* **2011**, *21*, 5897.
[29] K. Yang, X. Y. Huang, L. Y. Xie, C. Wu, P. K. Jiang, T. Tanaka, *Macromol. Rapid Comm.* **2012**, *33*, 1921.
[30] M. N. Tchoul, S. P. Fillery, H. Koerner, L. F. Drummy, F. T. Oyerokun, P. A. Mirau, M. F. Durstock, R. A. Vaia, *Chem. Mater.* **2010**, *22*, 1749.
[31] A. Maliakal, H. Katz, P. Cotts, S. Subramoney, P. Mirau, *J. Am. Chem. Soc.* **2005**, *127*, 14655.
[32] Z. Li, L. A. Fredin, P. Tewari, S. A. DiBenedetto, M. T. Lanagan, M. A. Ratner, T. J. Marks, *Chem. Mater.* **2010**, *22*, 5154.
[33] H. M. Jung, J. H. Kang, S. Y. Yang, J. C. Won, Y. S. Kim, *Chem. Mater.* **2010**, *22*, 450.
[34] K. Yang, X. Y. Huang, Y. H. Huang, L. Y. Xie, P. K. Jiang, *Chem. Mater.* **2013**, *25*, 2327.
[35] X. C. Pang, Y. J. He, B. B. Jiang, J. Iocozzia, L. Zhao, H. Z. Guo, J. Liu, M. Akinc, N. Bowler, X. L. Tan, Z. Q. Lin, *Nanoscale* **2013**, *5*, 8695.
[36] K. Yu, Y. J. Niu, Y. Y. Bai, Y. C. Zhou, H. Wang, *Appl. Phys. Lett.* **2013**, *102*, 102903.
[37] J. W. Xu, C. P. Wong, *Appl. Phys. Lett.* **2005**, *87*, 082907.
[38] L. Y. Xie, X. Y. Huang, B. W. Li, C. Y. Zhi, T. Tanaka, P. K. Jiang, *Phys. Chem. Chem. Phys.* **2013**, *15*, 17560.
[39] Y. Shen, Y. H. Lin, C. W. Nan, *Adv. Funct. Mater.* **2007**, *17*, 2405.
[40] Y. Shen, Y. H. Lin, M. Li, C. W. Nan, *Adv. Mater.* **2007**, *19*, 1418.
[41] Z. M. Dang, S. S. You, J. W. Zha, H. T. Song, S. T. Li, *Phys. Status Solidi A* **2010**, *207*, 739.
[42] S. Ducharme, *ACS Nano* **2009**, *3*, 2447.
[43] B. Balasubramanian, K. Kraemer, N. Reding, R. Skomski, S. Ducharme, D. Sellmyer, *ACS Nano* **2010**, *4*, 1893.
[44] Y. U. Wang, D. Q. Tan, *J. Appl. Phys.* **2011**, *109*, 104102.
[45] N. Guo, S. A. DiBenedetto, P. Tewari, M. T. Lanagan, M. A. Ratner, T. J. Marks, *Chem. Mater.* **2010**, *22*, 1567.
[46] N. Guo, S. DiBenedetto, D. Kwon, L. Wang, M. Russell, M. Lanagan, A. Facchetti, T. Marks, *J. Am. Chem. Soc.* **2007**, *129*, 766.
[47] L. A. Fredin, Z. Li, M. A. Ratner, M. T. Lanagan, T. J. Marks, *Adv. Mater.* **2012**, *24*, 5946.
[48] L. A. Fredin, Z. Li, M. T. Lanagan, M. A. Ratner, T. J. Marks, *Adv. Funct. Mater.* **2013**, *23*, 3560.
[49] L. A. Fredin, Z. Li, M. T. Lanagan, M. A. Ratner, T. J. Marks, *ACS Nano* **2013**, *7*, 396.
[50] H. Stoyanov, D. Mc Carthy, M. Kollosche, G. Kofod, *Appl. Phys. Lett.* **2009**, *94*, 232905.
[51] K. Yang, X. Y. Huang, M. Zhu, L. Y. Xie, T. Tanaka, P. K. Jiang, *ACS Appl. Mater. Interfaces* **2014**, *6*, 1812.
[52] L. Y. Xie, X. Y. Huang, K. Yang, S. T. Li, P. K. Jiang, *J. Mater. Chem. A* **2014**, *2*, 5244.
[53] L. Y. Xie, X. Y. Huang, Y. H. Huang, K. Yang, P. K. Jiang, *J. Phys. Chem. C* **2013**, *117*, 22525.
[54] L. Y. Xie, X. Y. Huang, Y. H. Huang, K. Yang, P. K. Jiang, *ACS Appl. Mater. Interfaces* **2013**, *5*, 1747.
[55] X. C. Pang, L. Zhao, W. Han, X. K. Xin, Z. Q. Lin, *Nat. Nanotechnol.* **2013**, *8*, 426.
[56] H. Z. Guo, Y. Mudryk, M. I. Ahmad, X. C. Pang, L. Zhao, M. Akinc, V. K. Pecharsky, N. Bowler, Z. Q. Lin, X. Tan, *J. Mater. Chem.* **2012**, *22*, 23944.
[57] M. Rahimabady, M. S. Mirshekarloo, K. Yao, L. Lu, *Phys. Chem. Chem. Phys.* **2013**, *15*, 16242.
[58] M. Molberg, D. Crespy, P. Rupper, F. Nuesch, J. A. E. Manson, C. Lowe, D. M. Opris, *Adv. Funct. Mater.* **2010**, *20*, 3280.
[59] I. Balberg, *J. Appl. Phys.* **2011**, *110*, 061301.